applied sciences

MDPI

Article

Evaluation of Noise-Reduction Techniques for Gas-Turbine Test Stands: A Preliminary Analysis

Laurentiu Cristea * and Marius Deaconu

National Research and Development Institute for Gas Turbines COMOTI, 220D Iuliu Maniu, 061126 Bucharest, Romania; marius.deaconu@comoti.ro
* Correspondence: laurentiu.cristea@comoti.ro

Abstract: Emphasizing the importance of acoustic attenuation in maintaining compliance with stringent noise regulations and enhancing workplace safety, this analysis covers theoretical and practical aspects of prediction methods used for the development of sound attenuators for gas-turbine testing stands. This paper presents a preliminary analysis and evaluation of the improvement of the Embleton method for projecting a noise attenuator for industrial applications, especially for gas-turbine test stands. While primarily focusing on the static acoustic behavior of the attenuator, certain considerations were also made regarding flow conditions, Mach number-dependent attenuation, pressure drop, and self-generated noise aspects to provide a comprehensive perspective on applying a suitable evaluation method. The study investigates different calculation methods for the assessment of noise reduction for linear and staggered baffles applied on a scaled reduced model of an attenuator. Thus, the critical parameters and development requirements necessary for effective noise reduction in high-performance gas-turbine testing environments will be evaluated in a downscaled model. Key factors examined include the selection of design parameters and configurations from various topological options (single, double, and triple parallel baffles vs. double and triple staggered baffles). Advanced computational methods, like analytic and finite-element analysis (FEM), are used to predict acoustic performance and evaluate the prediction method. Experimental validation is performed to corroborate the simulation results, ensuring the reliability and efficiency of the attenuator. The results indicate that an improved prediction method led to a better design for a sound-attenuator module, which can significantly reduce noise levels without compromising the operational performance of the gas turbine inside a test cell.

Keywords: baffle attenuator; gas-turbine stand; experimental validation; Embleton's method; anechoic chamber; rectangular duct flow

check for updates

Citation: Cristea, L.; Deaconu, M. Evaluation of Noise-Reduction Techniques for Gas-Turbine Test Stands: A Preliminary Analysis. *Appl. Sci.* **2024**, *14*, 5702. https://doi.org/10.3390/app14135702

Academic Editor: John S. Allen

Received: 29 May 2024
Revised: 20 June 2024
Accepted: 20 June 2024
Published: 29 June 2024

Copyright: © 2024 by the authors. Licensee MDPI, Basel, Switzerland. This article is an open access article distributed under the terms and conditions of the Creative Commons Attribution (CC BY) license (https://creativecommons.org/licenses/by/4.0/).

1. Introduction

Noise attenuators, commonly referred to as silencers, are integral to reducing acoustic emissions during gas-turbine testing. Their efficacy is influenced by various factors, including material properties, geometric configurations, and integration within the test-stand infrastructure. Despite their significance, comprehensive studies on the design and implementation requirements of these modules in gas-turbine testing environments are lacking. This study addresses this gap by conducting a thorough preliminary analysis of sound-attenuator modules. The objective is to establish a robust framework for the design and integration of sound-attenuator modules, ensuring optimal acoustic performance while maintaining the operational integrity of gas-turbine test stands. This analysis encompasses both theoretical approaches and practical considerations, employing advanced simulation techniques such as finite-element analysis to predict and enhance the acoustic attenuation capabilities of the proposed designs.

Experimental validations are performed to ensure the accuracy and reliability of our simulation results. By comparing theoretical predictions with empirical data, we identify

key areas for prediction-method improvement and potential innovations in attenuator technology. This paper not only contributes to the fundamental knowledge of noise attenuation but also provides valuable insights for engineers and designers involved in the development of medium gas-turbine testing infrastructure (source noise levels around 120 dB for turbofan engines and up to 160 dB for afterburning engines, according to Aerospace Recommended Practice SAE ARP5759/Acoustical Considerations for Engine Test Cell). Designing an acoustic attenuator for a gas-turbine test stand involves the use of analytical models based on empirical calculation relationships or advanced methods such as finite-element simulations. Each approach has its advantages and disadvantages: analytical methods provide quick results but are prone to high error margins, whereas the finite-element method offers greater accuracy but is time-consuming and resource-challenging. Both methods need precise input data to ensure the accuracy of the predicted results. Classic prediction methods mostly use analytic calculations for noise attenuation in rectangular ducts. Some of them have been proven through experimental validation, like in Vér's and Beranek's applications [1]. Such methods have some limitations, such as applying simple linear arrangements (only linear parallel arrangement) or not using the physical characteristics of the materials (density, porosity, rigidity). This is the reason why it would be necessary to apply advanced numerical methods in parallel with analytic ones in different topologies to validate a better design method. This is the main purpose of this article.

The improvement of transmission loss through pipe wrappings and enclosure walls, as well as the attenuation of sound propagating in ducts, involves various strategies and materials aimed at reducing sound-energy transmission through these structures, as studied by Bies and Hansen [2]. In this article, the acoustic parameters insertion loss and noise attenuation are evaluated using a method that is more appropriate for use in available testing conditions. A broadband low-frequency rectangular silencer with a sandwich plate was experimentally tested by Wang et al. [3], achieving a transmission loss of more than 10 dB across the entire frequency band. The same rectangular silencer with sandwich panels is also studied in this article but with different topologies. The propagation of sound in rectangular and other geometry section ducts was analyzed in detail by Erkan [4] through the mathematical analysis of sound propagation and radiation. A reactive perforated muffler was investigated numerically, experimentally, and analytically by Sumit et al. [5], resulting in transmission-loss data. Various internal configurations for silencers, including the effects of side-branch partitions, multi-chamber partitions, and their combined effects, were examined by Yu and Cheng [6].

Acoustic pressure radiation from a perforated region was studied by Wang et al. [7], who found that such areas can significantly reduce the pressures radiated from a duct outlet. The concept of perforated panels is used and numerically analyzed in this article. Numerical and experimental investigations were conducted by Zhou et al. [8], concluding that isotropic behavior was observed in perforated plates with circular holes under the square and triangular penetration pattern geometries also used in this article. Low-frequency tonal noise reduction was studied by Williams et al. [9], using dissipative and reactive elements in silencers, thus enabling reactive elements to function effectively over an extended low to medium frequency range. Terashima [10] used a finite-element approach to evaluate sound transmission loss in perforated silencers, concluding that discrepancies in sound transmission-loss results may be attributed to the viscous effects of sound-wave propagation and geometric imperfections. Kalita and Singh [11] performed an acoustic performance analysis of absorption materials used in sound attenuators, concluding that a type of glass wool (with a density of 24 kg/m^3 and flow resistivity of 14,000 Pa s/m^2) inserted in a muffler yielded the best transmission loss compared to rock wool, polyester, or melamine.

Experiments with parallel-baffled mufflers and perforated panels were conducted by Xiaowan Su [12], who created a testing stand and studied the transmission loss for various panel configurations. In his study, he did not use a staggered configuration; thus,

it was necessary to analyze it to be more appropriate for noise attenuation in gas-turbine test stands. Liu et al. [13] investigated noise reduction and the acoustic impedance of a ducted intake using a modified time-domain model instead of the classical transmission-loss model. Porous lamellas placed in a rectangular duct of an attenuator were evaluated numerically and experimentally by Li et al. [14], proving that acoustic attenuation is primarily due to viscous and structural dissipation. By contrast, in the present study, the viscous and structural dissipation through panels will be numerically investigated by applying impedance modification phenomena given by the perforation of a metal sheet.

This investigation acoustically and aerodynamically evaluates attenuators with parallel acoustic baffles made from mineral wool in both linear and staggered topologies within a rectangular duct by considering simple-, double-, and triple-baffled configurations. These configurations represent the concept and a downscaled version of a future noise attenuator to be incorporated into a gas-turbine test stand. Specialized literature on baffled noise attenuators provides calculation models that yield varying results [15]. In this study, an analytical method for calculating the attenuation of a baffle attenuator is investigated alongside the finite-element method, and the results of both methods are compared with experimental data. The study assesses the acoustic attenuation in three flow conditions—without flow, indirect, and reverse flow—by taking into consideration the influences of the convective effect on attenuation and the self-noise of the air passing through the baffles for all studied configurations. The analyzed configurations are also evaluated from a gas dynamic perspective to determine pressure loss, using both an empirical method and the finite-element method. To ensure the accuracy of the 2D simulation models, a comparative analysis between 2D and 3D models is conducted to establish if the 2D simulations can offer a balance between computational efficiency and accuracy.

2. Noise-Attenuation Assessment Embleton's Analytical Method

To identify a calculation model for the acoustic attenuation of a lamellar attenuator, both the analytical method developed by Embleton [16] and the finite-element method using MSC Actran software version 19 were employed. The finite-element method with Actran involves calculating acoustic propagation at each point in the grid, accounting for air impedance, reflections from solid and absorbent objects, propagation through porous materials, and free-field acoustic wave propagation. In the Embleton method, a parallel baffle silencer operates as a type of lined duct, wherein each passage between the baffles acts as an individually lined duct. The transmission losses in such systems arise from the sound absorption within the porous lining as the sound waves travel through the duct. When the cross-sectional area of the lining approaches the size of the open area through which the sound travels, additional losses occur due to wave reflections at the lining's end, enhancing the silencer's effectiveness as a reactive silencer. Embleton's method simplifies by assuming a plane-wave propagation, which eases calculations but does not perfectly reflect the physical reality, hence the necessity of going deeper into the phenomenon. This approach allows for the estimation of sound attenuation, significantly accounting for lower modes that persist longer in the lining. The simplicity of Embleton's graph-based method consists of facilitating the prediction of total attenuation by requiring only a few parameters: baffle width, spacing, length, and sound wavelength. Also, the method presented by Embleton does not approach the staggered configuration, which would be a proper solution to use on a turbojet test stand. By studying this configuration of staggered baffles, a modification of the prediction formula is compulsory, and it will be further applied for evaluation in this article.

Figure 1a presents schematically the geometric parameters of the attenuator and the noise-attenuation curves used by Embleton. The parameters necessary for calculating the attenuation include the width of the lamella t, the distance between the baffles ly (which is the width of the air channel), and the baffle length L. These parameters are used to calculate the percentage of the open area (POA [%]) of the attenuator, the ratio ly/λ (where λ is the wavelength), and the speed of sound in air c. Based on these data, applied to

Equation (1), the attenuation curves A_{ly} from Figure 1b are consulted to complete the Embleton method [16]. Original works like Beranek's "Noise and Vibration Control" (1971) mostly used Embleton's method, and the recent ones are referenced to the Galaitis and Vér methods, which are applied for dissipative noise silencers for parallel baffles [16] Ingard developed a software-based prediction method for the calculation of noise attenuation, transmission loss, and insertion loss, but only for lined ducts [17], without taking into consideration a staggered arrangement of the baffles.

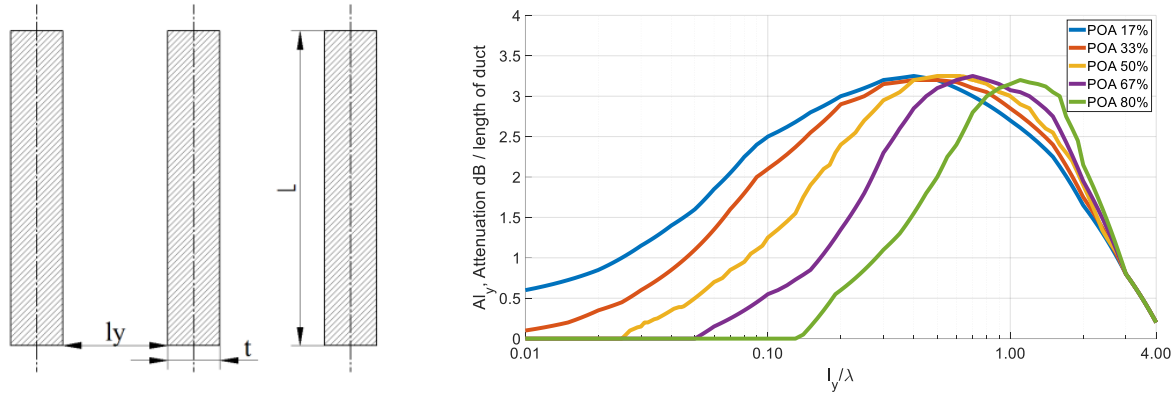

(**a**) (**b**)

Figure 1. Embleton method—parameters: (**a**) Schematic duct geometry of the attenuator; (**b**) noise curves used for attenuation prediction (Embleton).

Based on the open area, the corresponding Al_y curve is selected and then multiplied by the ratio L/l_y, yielding the acoustic attenuation of the attenuator, as described by Equation (1).

$$Attenuation = Al_y * \frac{L}{l_y} \text{ [dB]} \quad (1)$$

The open area is computed using the relation POA = $l_y/(l_y + t) \times 100$. For intermediate porosities, values from the graph can be interpolated. The frequency can be determined using Figure 1b, where $f = (l_y/\lambda) \times (c/l_y)$.

The relationships for acoustic attenuation, as presented by Embleton [16] in the form of Equation (2), can be adjusted according to the airflow velocity between the baffles according to Equation (2). This relationship takes into account the influences of convective phenomena and the self-noise of the baffles on acoustic attenuation

$$Attenuation_{flow} = A\left(1 - 1.5 * M + M^2\right) \text{ [dB]} \quad (2)$$

where A is the noise attenuation without flow, and M is the Mach number, and it is valid only for $-0.3 < M < 0.3$ (with the physical meaning of reverse and direct flow condition relative to the noise location) [18].

The main disadvantage of the Embleton method is that the calculation model does not account for changes in the structural properties of the mineral wool, even though density is a known critical parameter that significantly influences acoustic attenuation by shifting the absorbed frequency. Another disadvantage is that this method neglects the properties of the perforated panel. Additionally, the calculation model is only applicable to simple attenuator geometries with linear and parallel baffles. However, the main advantage of this method is that it does not require complex software or significant computing resources, resulting in a short turnaround time to obtain results.

Noise attenuation is an intrinsic acoustic parameter of an attenuator. Another acoustic parameter is self-noise, manifested by noise generated from the flow interaction with the baffles. The noise generated by flow has different characteristics, depending on the direction of the flow, as is the case of the gas-turbine test cell, where sound waves travel

in the direction of flow (exhaust domain) and in the opposite direction of flow (intake domain). Figure 2 presents an evaluation of the noise attenuation produced by a single-level attenuator and the influences of airflow through the baffles using Embleton's formulas. It proves that, compared to the static case without flow, a Mach number of 0.3, whether positive or negative, leads to a decrease or increase in attenuation by up to 10 dB. The Embleton method was used to calculate the noise attenuation and the flow correction using Equation (2). The geometrical parameters of the attenuator were ly = 0.1 m, t = 0.1 m, and L = 0.6 m.

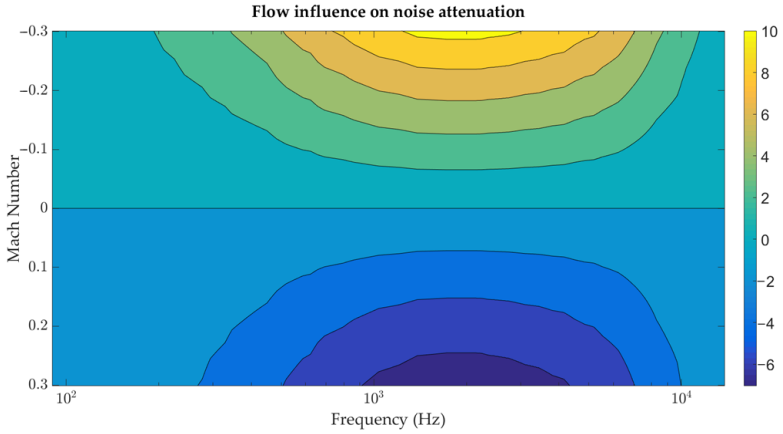

Figure 2. Noise attenuation of a single-level attenuator as a function of the Mach number.

Flow-induced noise, also known as self-noise, is an inevitable consequence of fluid movement and an underlying factor to consider in any system involving airflow. If self-noise becomes excessive, redesigning the baffle silencer becomes necessary, as other noise-reduction methods might have limited effectiveness. Excessive self-noise is a result of a high level of turbulence, which has an unwanted and possible dramatic consequence in the test-cell environment, leading to subsonic drops or chocking of the engine, for example. In this study, for a more accurate determination of self-noise, which takes into consideration also the temperature and the distribution of perforation areas, an analytical method proposed by Munjal [19] is used for the calculation of self-noise for the linear version of attenuators, and the results are compared with results from the finite-element method (FEM). Munjal's method is employed to estimate the acoustic power level generated by flow-induced noise in systems with baffles, such as noise attenuators. Equation (3) is used in this evaluation method:

$$L_{w,self} = 10\log_{10}\left(2.16 \times 10^5 * U^{5.4}.\frac{A_b}{(T+273)^{2.27}\left(\frac{POA}{100}\right)^4}\right)\text{[dB]} \quad (3)$$

where U is the flow velocity [m/s], A_b is the front area of the baffles [m^2], T is the air temperature [°C], and POA is the percentage of the open area of the attenuator [%]. Self-noise is highly dependent on flow velocity. An increase in flow velocity will significantly impact the acoustic power level, as the power of flow-induced noise increases exponentially with the flow velocity.

3. Noise-Attenuation Assessment—Finite-Element Method

The validation of the Embleton model and the finite-element method was conducted by comparing the results with the experimentally obtained values. For this purpose, an experimental stand was set up to test lamellar attenuators. The finite-element method involves creating a geometric model of the test bench, as presented in Section 3, meshing it, applying boundary conditions, and then conducting the acoustic analysis. The numerical scheme considers phenomena such as acoustic propagation in gaseous and porous media, acoustic reflections and absorptions, and the propagation of acoustic waves in a free

field. Figure 3 presents the internal geometry of the test bench. To reduce computational time, a 2D simulation was performed. The applied boundary conditions are as follows: the blue line represents the boundary condition of acoustic pressure, with a pressure of 100 Pa applied along it, representing the acoustic source; the black lines represent the walls of the test bench, modeled as perfectly reflective surfaces; the red line represents the free-field boundary condition, allowing the propagation of acoustic waves from inside the domain to the exterior, without returning to the computational domain; the green lines represent the perforated panel with a porosity of POA = 30%, hole diameter φ = 4 mm, panel thickness b = 0.5 mm, corresponding to the tested structure. The blue-colored surface inside the test bench represents the fluid domain with a sound speed c = 340 m/s and density ρ_0 = 1.225 kg/m^3, while the yellow domain represents the mineral wool for which was introduced a flow resistivity σ = 30,000 Rayls/m, simulating a mineral wool density of approximately 80–100 kg/m^3. In the acoustic analysis for the calculation of acoustic absorption and interior propagation through the porous material, the Delany–Bazley calculation model was used [20,21]. The Delany–Bazley method is used to predict the acoustic properties of porous materials in terms of sound absorption and attenuation characteristics. The method estimates complex wave numbers and the characteristic impedance of porous materials based on flow resistivity. The following equations describe the acoustic characteristics:

$$Z_c = \rho_0 c \left(1 + 0.0571 \left(\frac{\rho_0 f}{\sigma}\right)^{-0.754} - j0.087 \left(\frac{\rho_0 f}{\sigma}\right)^{-0.732}\right) \quad (4)$$

$$K_c = \frac{\omega}{c}\left[1 + 0.0571 \left(\frac{\rho_0 f}{\sigma}\right)^{-0.7} - j0.189 \left(\frac{\rho_0 f}{\sigma}\right)^{-0.595}\right] \quad (5)$$

where σ is the flow resistivity of the fluid, f is the propagation frequency, ρ_0 the density of the fluid, and ω is the angular frequency. A Delany–Bazley method was applied by Won and Choe [22] to analyze the transmission loss of a partitioned rectangular duct in numerical simulations and experimental validation, although without considering the flow condition.

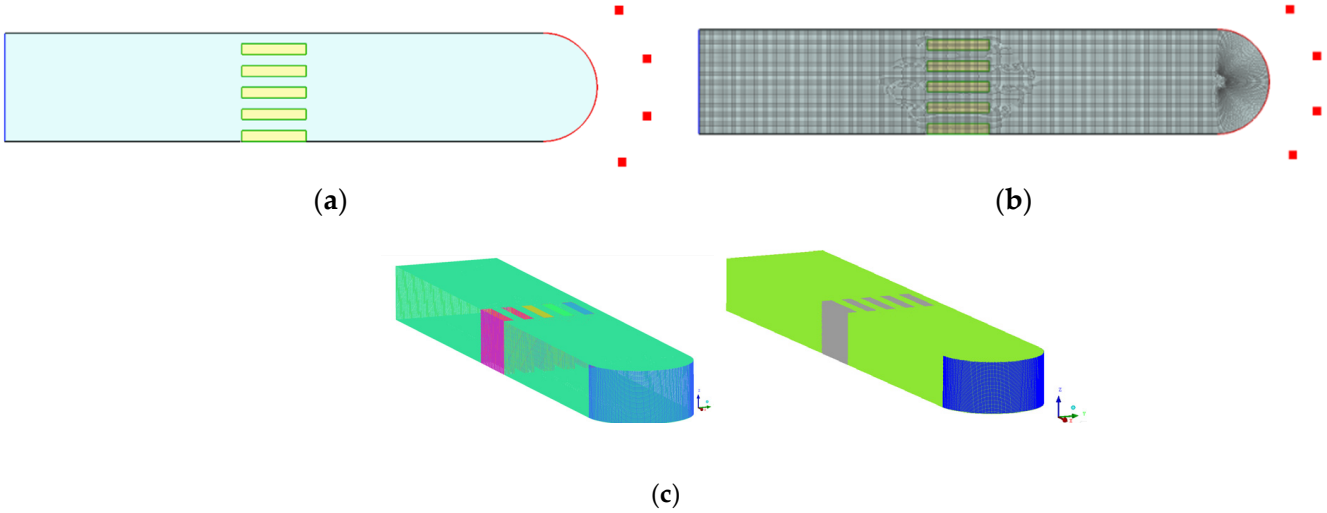

Figure 3. Test-bench geometry and computational grid: (**a**) top view of geometry with a boundary condition—baffle (yellow), acoustic domain (light blue), free domain (red); (**b**) 2D mesh (element size of 7 mm)—baffle (yellow), free domain (red); (**c**) 3D mesh (element size of 7 mm)—baffle (grey), acoustic domain (green), free domain (blue).

The red dots indicate the positions of the microphones used in the tests to evaluate the attenuation capacity of the silencers. The mesh, shown on the right side of Figure 3, is composed of rectangular elements with a maximum dimension of 8 mm, corresponding to

a maximum analysis frequency of approximately 10 kHz. A mesh with quadratic elements was utilized with a rule of a minimum of four elements per wavelength, which must be followed to accurately capture the propagation of the acoustic wave. As observed in Figure 3b, the employed mesh contains quadratic elements, and it is partially structured in the regions adjacent to the baffles. For the porous domain, a structured mesh was generated using quadratic elements with an element size of 7 mm. For the 2D configuration presented in Figure 3b, 82,000 elements resulted as optimum. A 3D mesh with 5,760,000 elements was also generated for the first configuration of baffles to compare the 2D and 3D results and estimate the confidence in using the 2D simulation for time and computational saving. As in the case of 2D simulation, the same boundary conditions were applied for the 3D simulation. Figure 3 presents a comparative graph with radiated acoustic power resulting in a 2D simulation versus a 3D one. This comparative presentation was carried out to evaluate the similitude between them by taking into consideration the restriction introduced by a 2D concept as compared to a 3D one.

Figure 4 highlights that the differences in radiated power outside of the test bench are similar, with small differences appearing at low and high frequencies.

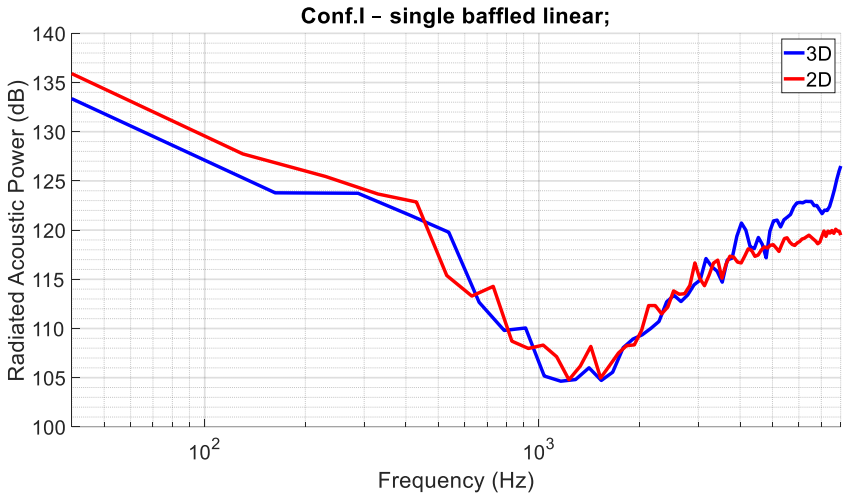

Figure 4. Comparison of simulated radiated power, 2D and 3D results [dB].

The acoustic pressure fields, as presented in Figure 5, are similar in 2D and 3D representations, so we can conclude that the 2D simulation is sufficiently accurate, as compared to the 3D one, and that it could be used as a good option to obtain correct results, by saving computational and time resources, especially when a flow-acoustic analysis is needed.

The procedure for evaluating acoustic attenuation, both in numerical simulations and measurements, involves measuring the acoustic pressure at four points outside the test bench, which are positioned radially around the free end of the stand and then logarithmically averaging them. The first measured configuration is without an acoustic baffle inside the duct, resulting in an average sound pressure $\overline{L_{p1}}$. This is followed by the introduction of baffles and subsequent measurement, resulting in an average sound pressure $\overline{L_{p2}}$. The difference between the two average noise levels represents the acoustic attenuation (insertion loss—*IL*) in dB of the tested configuration

$$IL = \overline{L_{p1}} - \overline{L_{p2}}\ [\text{dB}] \tag{6}$$

The main advantage of this numerical method is its ability to model complex attenuator shapes and incorporate various parameters of the mineral wool and perforated panels. However, the computational cost increases with model complexity.

The primary disadvantage of this method is the significant computing resources required, particularly for 3D simulations. Additionally, the development of the CAD model and the computational grid can be time-consuming.

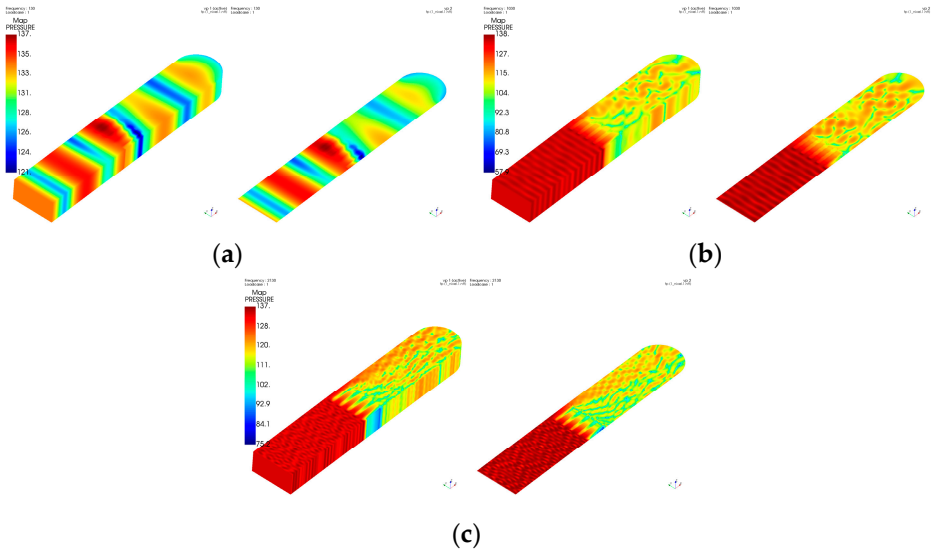

Figure 5. Comparison of acoustic fields in 2D vs. 3D simulations: (**a**) 130 Hz, (**b**) 1030 Hz, (**c**) 2130 Hz.

4. Test-Bench Description

A downscaled model was tested under anechoic conditions to evaluate the attenuator's performance. The testing stand, depicted in Figure 6, consists of a duct with a length of L_{duct} = 5.7 m and a rectangular cross-section with a width of L_{duct} = 1 m and a height of h_{duct} = 0.5 m. One end of the stand is closed, while the other remains open. At the closed end, inside the testing bench, an acoustic source (omnidirectional acoustic source Bruel & Kjaer 4292-L (Brüel & Kjær, Nærum, Denmark)) was placed approximately 2 m away from the baffles, emitting pink noise in the frequency range of 50–16,000 Hz, with an overall acoustic pressure level of approximately 125 dB, thus creating a strong diffuse field inside. At the open end, approximately 2 m away from it, four microphones were placed, according to Figure 6, and the acoustic spectra were logarithmically averaged. The stand was constructed from 18-mm-thick chipboard panels with a density of 680–740 kg/m^3. To stiffen the test bench and reduce acoustic transmission through its walls, the chipboard panels were doubled. To minimize unwanted noise, the tests were conducted inside the anechoic chamber of INCDT COMOTI (Bucharest, Romania). The anechoic chamber (Figure 6a), designed and executed according to ISO 3745 [23] requirements, has a volume of 1200 m^3, with dimensions 15 × 10 × 8 m and with a wall absorption coefficient of 99%, in a frequency range of 150 Hz up to 20,000 Hz [24].

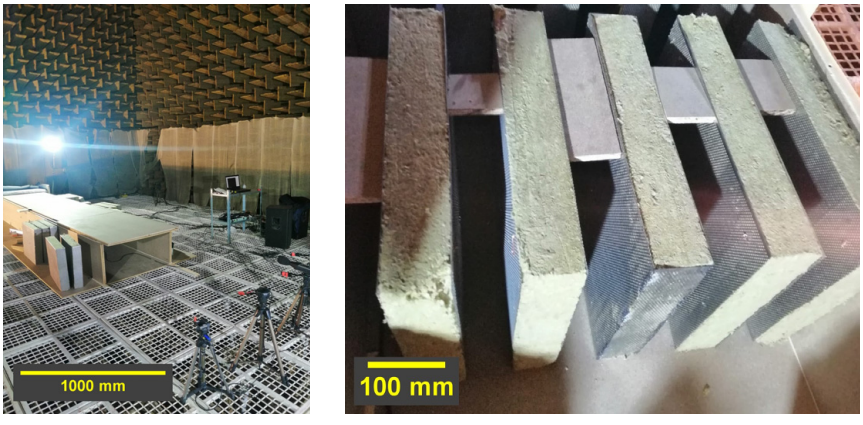

Figure 6. Test bench inside the anechoic room and microphone locations: (**a**) Test bench in the anechoic room; (**b**) Perforated sandwich panel baffle inside the test bench.

The baffled sandwich panels were made from basalt mineral wool, with a density of 80 kg/m^3, and a steel perforated sheet with a percentage of openings of POA = 30%, hole diameters φ = 4 mm, and panel thickness b = 0.5 mm, baffle length L = 0.6 m, baffle height h = 0.5 m, and baffle width l = 0.1 m, as presented in Figure 6b.

The literature in the field has shown that interleaving or staggering baffles leads to improved acoustic performance. Therefore, this study analyzed two attenuator models with staggered baffles and compared their acoustic attenuation results to linear baffle attenuators of the same total baffle length. Configurations II and IV, as well as configurations III and V, use the same total baffle length. However, in Configurations IV and V, the baffles are staggered. Figure 7 presents schematic representations of the tested attenuator configurations. Configuration I consisted of a single attenuator section with parallel baffles.

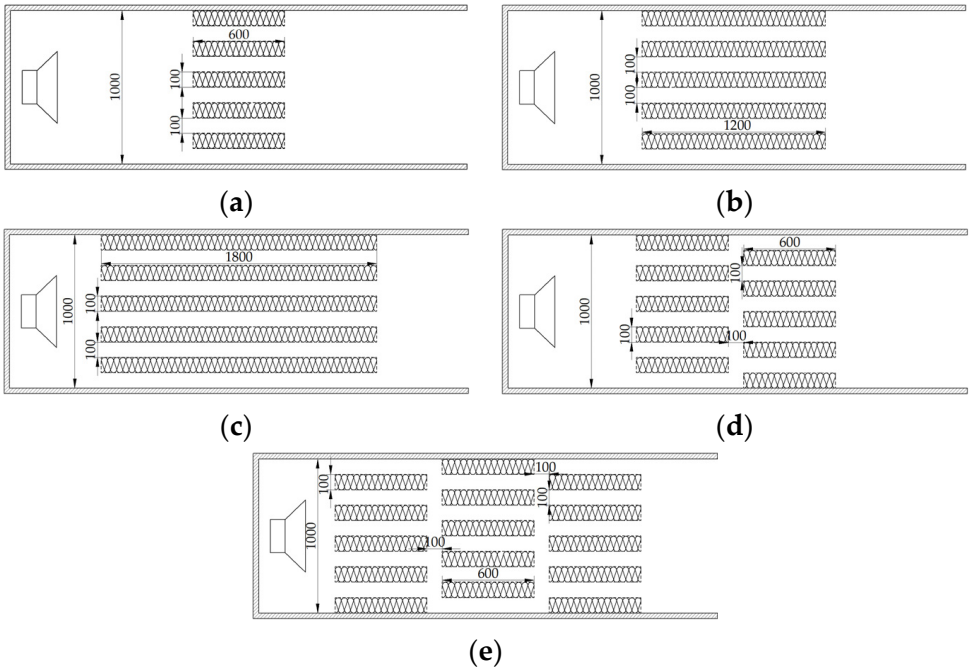

Figure 7. Drawings of the tested configurations: (**a**) Conf. I—single baffled_linear; (**b**) Conf. II—double baffled_linear; (**c**) Conf. III—triple baffled_linear; (**d**) Conf. IV—double baffled_staggered; (**e**) Conf. V—triple baffled_staggered.

The second configuration involved testing of two baffle sections placed end to end. Similarly, the third configuration consisted of three baffle sections placed end to end. In contrast, the fourth configuration employed two staggered sections, while configuration V utilized three staggered baffle sections.

For all configurations, the distance between individual baffles and the staggered sections was maintained at l_s = 0.1 m. Additionally, the exposed edges of the attenuators (those facing the acoustic waves) were covered with perforated panels, as presented in Figure 8.

In the present study, for the evaluation of Configurations IV and V with staggered topology, an adaptation of Embleton's method is proposed to account for the intercalated (staggered) arrangement of the baffles. Since Embleton did not present a calculation method for staggered baffle configurations, we used the calculation for the linear version and modified the formula to address the differences between the calculated and measured results. The attenuation correction for the staggered baffle configuration (Figure 9) includes three factors: l_c—distance addition correction, l_s—distance between two levels of baffles, and l_y—air channel width between baffles. It is considered that in the propagation path of the acoustic wave, in the case of intercalated lamellae, it travels a greater distance l_c, which is defined as follows:

$$l_c = n\frac{l_y}{\cos(\phi)}\ [\mathrm{m}] \tag{7}$$

where n is the number of baffled levels in staggered topology.

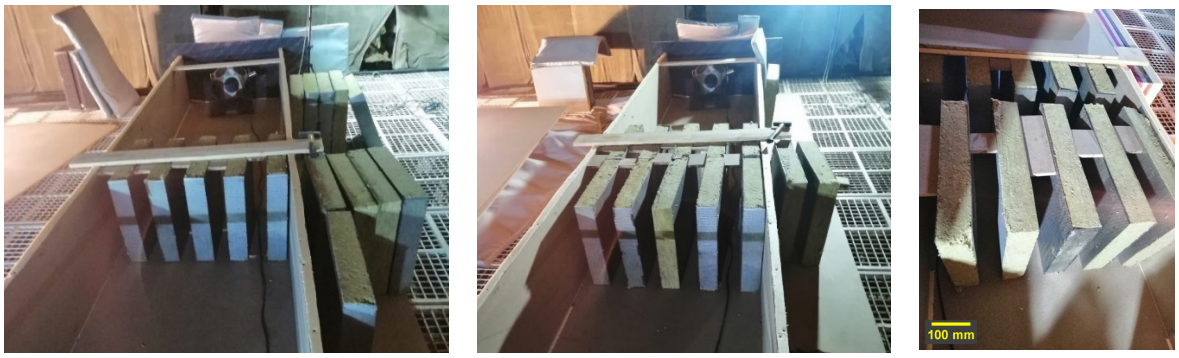

(**a**) (**b**) (**c**)

Figure 8. Panel arranged in various topologies: (**a**) Conf. I—single baffled_linear; (**b**) Conf. II—double baffled_linear; (**c**) Conf. III—triple baffled_linear.

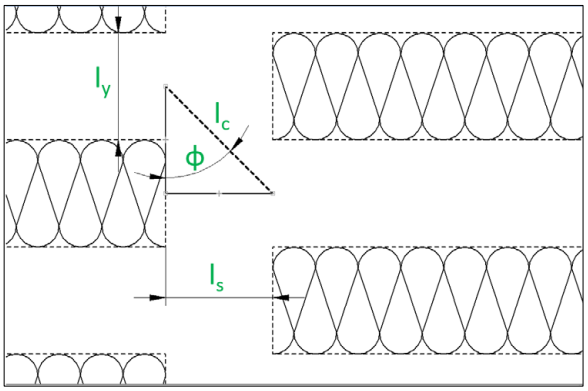

Figure 9. Attenuation correction in staggered baffles configuration.

Embleton proposes the use of silencers with a staggered baffle arrangement, as shown in Figure 9. This design eliminates straight paths for sound waves to travel through the baffles, potentially leading to improved attenuation at higher frequencies. However, Embleton's research [16] is focused on parallel-baffled attenuators, and it did not provide prediction methods for staggered configurations. Consequently, this study proposes an adaptation of Embleton's method specifically targeted to staggered topologies.

5. Pressure Loss and Self-Noise Evaluation

Pressure loss, which refers to the reduction in air pressure as air flows through the duct system, was also evaluated for all configurations. This phenomenon occurs due to friction and turbulence created by internal surfaces or any acoustic treatments within the duct. Sound-absorptive materials, such as mineral wool and perforated steel sheets, increase the roughness of the duct's internal surface, thus causing more friction between the air and the duct walls. Variations in duct cross-sectional area, designed to enhance noise attenuation by mitigating the beaming effect, can cause pressure changes and contribute to overall pressure loss. Excessive pressure drops can lead to additional noise, and compensatory higher flow speeds may result from excessive pressure drops.

The effect of sound on rectangular plates placed within the flow has been studied by Welsh and Parker [25], who found that shear layers attach to the leading edge in the center of vorticity and close to the boundary layer. Yu et al. [26] demonstrated the influence of rectangular geometries with different aspect ratios (ranging from 0.3 to 7) placed within the flow through extensive simulation and proving their impact on the flow field. The influence of different geometries of edges on the noise induced by flow was investigated by

Mohany and Shoukry [27], who concluded that rectangular edge geometries with 0.5 aspect ratios show a significant increase in flow-excited acoustic pressure. Tang [28] investigated the sound produced by a low-Mach vortex flow on a two-dimensional splitter, concluding that the sharp edge in the flow does not affect acoustic scattering. Noise attenuation of a rectangular duct with a perforated panel liner under one-direction flow conditions was studied by Zhang and Cheng [29] using the transfer functions method and experimental validation. In our case, we will study the attenuation in direct-end reverse-flow conditions, similar to intake and exhaust application cases. The following Almgren formula [15] is used to calculate the pressure drop in a single-baffled parallel attenuator with different length L of the baffles:

$$P = \frac{\xi \rho v_b^2}{2} + \frac{\lambda_{perf} L \rho v_b^2}{2 d_h} + \frac{\rho (v_b - v_0)^2}{2} \quad (8)$$

where the local loss coefficient $\xi \approx 0.1$ and friction coefficient $\lambda_{perf} \approx 0.05$ (0.05 for smooth walls and 0.1 for rough walls), and d_h is the hydraulic diameter.

The first term from Equation (8) represents the pressure loss caused by the inlet and outlet effects of the flow through the baffles; the second term represents the pressure loss due to friction along the walls of the channel, and the last term is the pressure loss due to changes in air velocity. The pressure drop occurs at the entry and exit of the baffle zone. Subsequently, the pressure drop for all linear configurations was analyzed using Equation (8) and compared with the results obtained from the Ansys Fluent version 15.0 software. Additionally, the staggered configurations were analyzed only with FEM. The boundary conditions introduced were an airflow rate of 6.125 kg/s defined at the inlet, corresponding to a speed of 10 m/s. Atmospheric pressure was applied at the outlet, assuming the gas to be ideal to account for density variations, and the $k - \varepsilon$ turbulence model was utilized. A steady-state flow analysis was conducted for these computations. The pressure loss was computed as the difference between the total pressure of the inlet and outlet. Based on the flow field, the noise power level inside the attenuator was computed using the Fluent acoustic software version 15.0 module, which is based on Proudman's formula [30]. Computational fluid dynamic (CFD) software was also used by Cai and Mak [31] to study a prediction method for flow-generated noise in air ducts produced by turbulent interaction between airflow and structural elements, such as baffles, to evaluate the radiated sound power, using an impact factor. In our article, we will numerically evaluate the radiated sound power inflow conditions for geometries more dedicated to real applications, like inlet and exhaust attenuators for gas-turbine test stands.

6. Results

6.1. Noise-Attenuation Assessment—Without Flow

The following section presents the acoustic results obtained from the test-bench measurements and the application of the two previously described methods. The following images illustrate the test results for various attenuator configurations. As shown in the graph in Figure 10, attenuation rapidly decreases at higher frequencies. This phenomenon, described by Embleton as the "beaming effect", occurs because high-frequency sound waves tend to travel directly through the gaps between the baffles. Consequently, they bypass the sound-absorbing material. Embleton suggests that high frequencies are not effectively absorbed due to this direct path. Instead of interacting with the absorptive material, the sound waves essentially travel the gaps with minimal influence, avoid absorption, and continue to propagate. This effect does not take place in a staggered configuration, where the insertion loss is higher at high frequencies.

When analyzing Figure 10, we see that Embleton's method generally aligns with the attenuation curves. However, a sharp decrease in predicted attenuation becomes evident at higher frequencies. The experimental results demonstrate that even for configurations with linearly arranged baffles, high-frequency acoustic waves (>6 kHz) undergo significant

acoustic attenuation; finite-element numerical simulations capture acoustic attenuations at high frequencies very well.

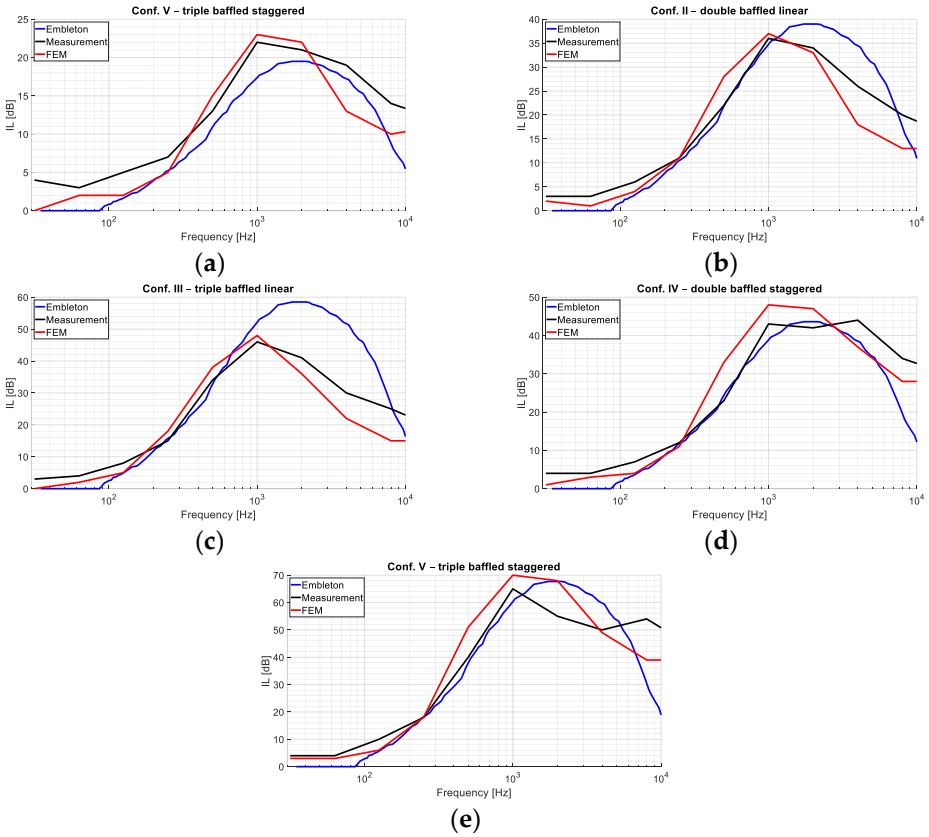

Figure 10. Comparison of the insertion loss IL [dB] results between measurements and numerical modeling: (**a**) Conf. I—single baffled_linear; (**b**) Conf. II—double baffled_linear; (**c**) Conf. III—triple baffled_linear; (**d**) Conf. IV—double baffled_staggered; (**e**) Conf. V—triple baffled_staggered.

We can mention that while simulations and measurements show the maximum attenuation peak centered around 1.5 kHz, the Embleton curve has its central frequency around 2 kHz. This shift of approximately 500 Hz is mainly due to the characteristics of the mineral wool of which the baffles are made. As we have already mentioned, Embleton's method ignores any changes in the density of the mineral wool. In the case of the attenuator configurations with linearly arranged baffles, the numerical simulations prove a high degree of fidelity to the measurements. However, Embleton's method tends to overestimate attenuation as the length of the attenuator increases.

For the staggered baffle configuration, the finite-element method predicts higher attenuation values than the measurements. This difference likely arises from two factors. First, the CAD model assumes perfect baffle positioning, whereas real-world installations may involve slight deviations due to manufacturing tolerances or assembly processes. These deviations can introduce imperfections that reduce the effectiveness of the baffles. Second, high attenuation in staggered baffle configurations can make measurements susceptible to noise from collateral sound paths. This additional noise can contribute to lower measured attenuation values. One last aspect to note is that numerical simulation achieves good correlation even at low frequencies, which is very important, especially in applications where such attenuators are used.

Figure 11 presents a comparison graph of the average insertion loss for all configurations investigated in this study. Since the primary focus of this research was to identify the optimal configuration for a sound attenuator in a gas-turbine test stand, a three-baffle staggered arrangement emerges as the most suitable choice.

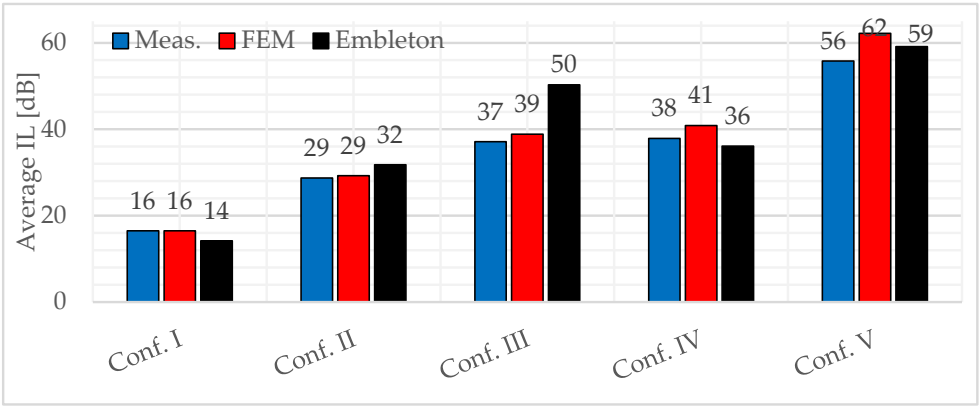

Figure 11. Averaged insertion loss for the analyzed configurations of the attenuator.

Figure 12 presents a comparison of sound-pressure levels obtained using Actran software [32] for a linear three-baffle configuration and a staggered three-baffle configuration. The results demonstrate a more attenuated acoustic field within the staggered baffle variant compared to the linear one. Consequently, the staggered configuration appears to be a more suitable choice for the final test-stand application. The acoustic fields reveal another important consideration: even though all channels have a width of 0.1 m, the marginal channel with one reflective wall allows for sound leakage. Therefore, in the final application, it is crucial to ensure that the duct walls are acoustically treated.

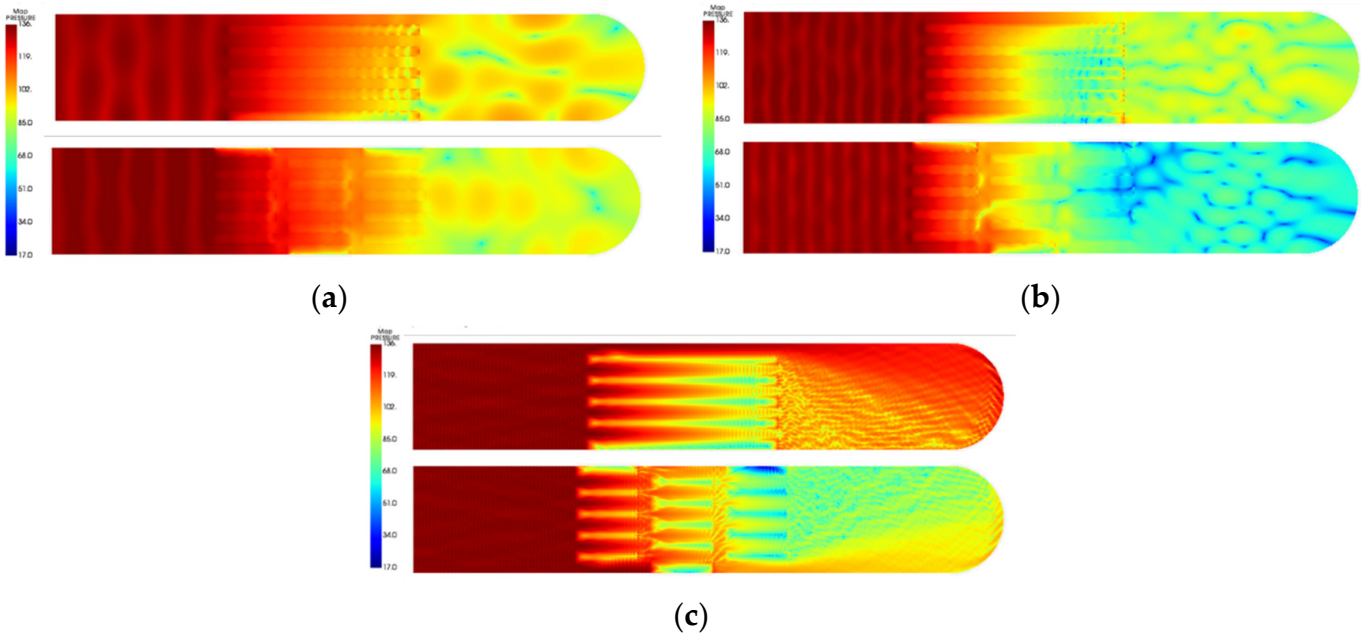

Figure 12. Acoustic field inside linear and staggered configurations—sound-pressure level [dB]: (**a**) 500 Hz; (**b**) 1000 Hz; (**c**) 5000 Hz.

6.2. Acoustic Attenuation with Convective Flow Phenomena

To evaluate the attenuation of an attenuator, it is necessary to consider the convective phenomena caused by the airflow within it. These phenomena, which affect the propagation of sound by modifying the properties of the propagation medium, such as sound velocity and density, can be assessed using Actran software by introducing the flow field, specifically the velocity and density fields.

In Figure 13, we show the velocity, density, and pressure fields in direct and reverse flow through the domains. The simulations indicate that some domains of variable densities appear due to the flow conditions, which have important effects on sound propagation,

with the baffle region acting as an interface with different acoustic impedance. Thus, the direct flow creates a higher-density domain in front of the baffles, where, by applying a direct acoustic field, a higher attenuation than in the static field or the inverse flow condition is obtained. Along this simulation, a flow of 100 m/s (M ≈ 0.3) in the baffle channels was considered to emphasize the variation of densities between distinct domains.

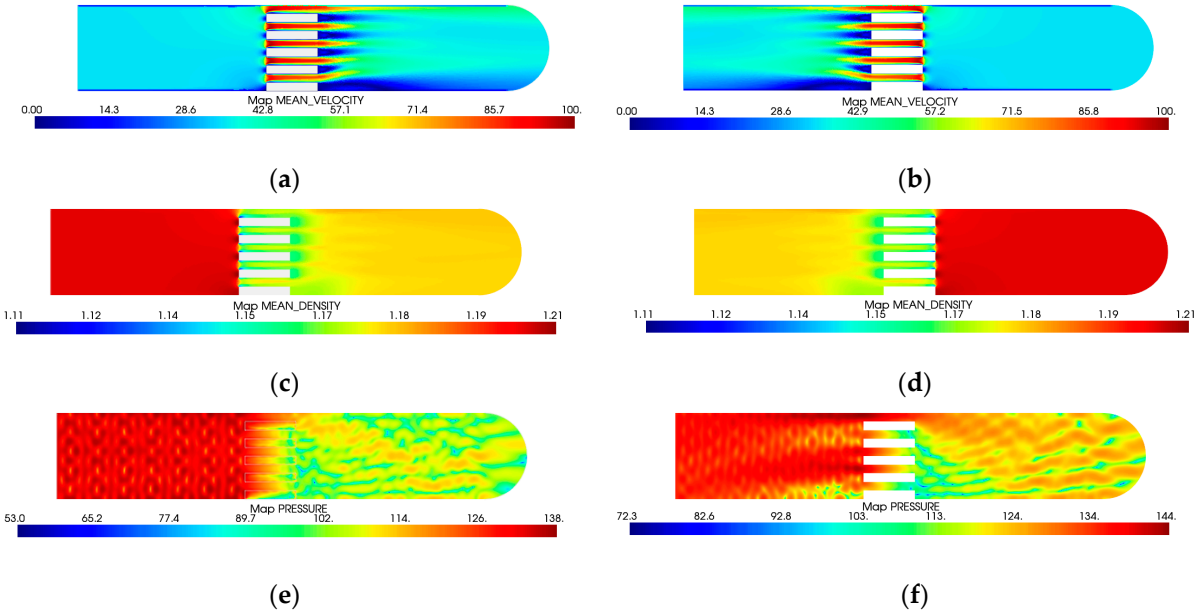

Figure 13. The influence of flow on the sound-pressure field: Mean air velocity ((**a**)—direct, (**b**)—inverse flow) [m/s], mean air density ((**c**)—direct, (**d**)—inverse flow) [m/s], and sound-pressure level ((**e**)—direct, (**f**)—inverse flow) [dB], fields.

Figure 14 shows the attenuation graphs obtained after FEM simulations. A higher attenuation in the case of a direct flow condition can be noticed, as compared to static and inverse flows, due to a passage from a higher-density domain to a lower-density one, and also, a frequency shift is revealed for all three cases due to the Doppler effect.

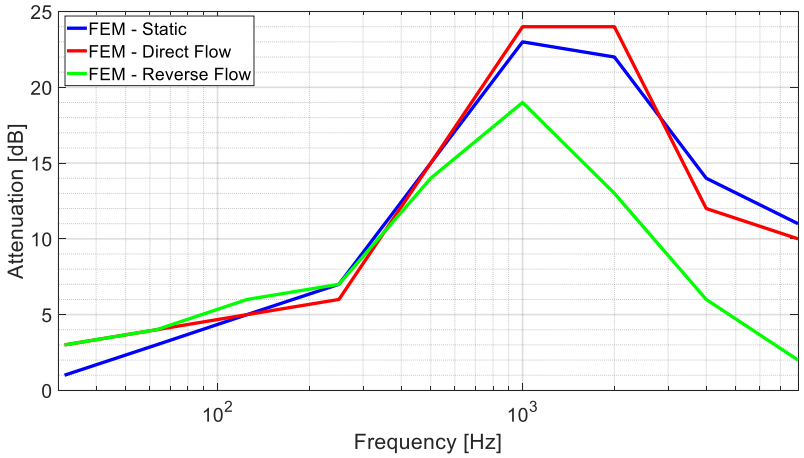

Figure 14. Influence of flow on sound attenuation—FEM method [dB].

6.3. Pressure Loss and Self-Noise Assessment

Table 1 presents the pressure loss for each analyzed configuration that used the Algrem [15] analytical method concurrently with the numerical method. The pressure loss was calculated at an inlet velocity of 10 m/s, resulting in an air velocity of approximately 30 m/s in the case of linear baffles and 40 m/s for staggered baffles. The pressure loss for

the staggered baffles was exclusively computed using the finite-element method (FEM) due to inherent limitations in the Algrem method.

Table 1. Pressure loss for each configuration—air velocity at a 10 m/s inlet.

Configuration	Pressure Loss [Pa]	
	Analytic	FEM
Conf. I—single baffled_linear configuration	124	164
Conf. II—double baffled_linear configuration	154	175
Conf. III—triple baffled_linear configuration	184	191
Conf. IV—double baffled_staggered configuration	-	446
Conf. V—triple baffled_staggered configuration	-	737

Linear configurations show lower pressure losses as compared to the staggered configurations. Staggered configurations generate significantly higher pressure losses due to the increased flow complexity and stronger interactions between the jets and deflector surfaces.

Figure 15 shows the pressure and velocity field inside the attenuator.

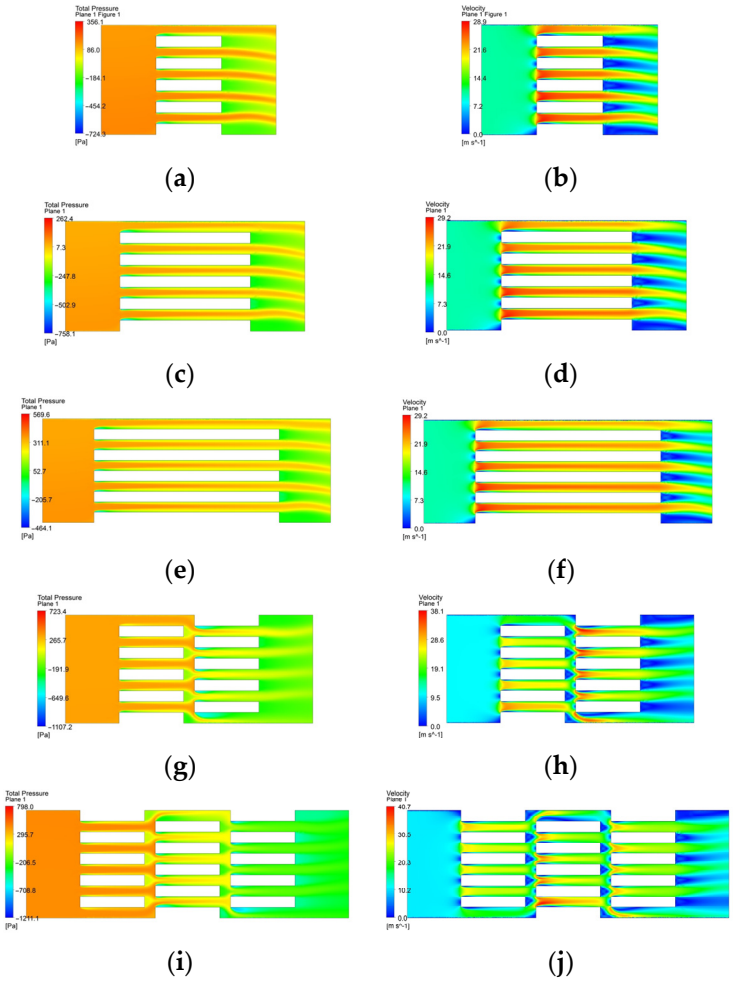

Figure 15. Flow fields inside the attenuator: (**a**) pressure field—Conf I; (**b**) velocity field—conf I; (**c**) pressure field—Conf II; (**d**) velocity field—Conf II; (**e**) pressure field—Conf III; (**f**) velocity field—Conf III; (**g**) pressure field—Conf IV; (**h**) velocity field—Conf IV; (**i**) pressure field—Conf V; (**j**) velocity field—Conf V.

The single-baffled linear configuration shows the lowest pressure loss among all configurations analyzed. The close agreement conformity between Almgren's and FEM results (124 Pa vs. 164 Pa) suggests a reliable estimation of pressure loss for this simple configuration. By adding a second baffle in a linear arrangement, the pressure loss increases slightly compared to the single-baffle configuration. The results from Almgren and FEM are again quite close (154 Pa vs. 175 Pa), indicating a consistent and predictable increase in pressure loss due to the additional baffle. When a third baffle is introduced, the pressure loss continues to increase, but the effect is not as significant as might be expected. The close match between Almgren and FEM results (184 Pa vs. 191 Pa) shows that the linear addition of baffles has a diminishing effect on increasing pressure loss. The double-baffled staggered configuration results in a significant increase in pressure loss compared to the linear configurations. The FEM analysis shows a pressure loss of 446 Pa, which is substantially higher than the double-baffled linear configuration. This indicates that the staggered arrangement causes more turbulence and resistance to airflow. The triple staggered configuration shows the highest-pressure loss at 737 Pa, as shown in the FEM analysis. This configuration introduces the most significant turbulence and obstruction of airflow, leading to the highest energy loss in all configurations analyzed.

Square-edged baffles have a significant negative impact on the airflow or fluid flow. Their sharp-edged design causes flow separation at the deflector inlet, leading to the formation of recirculation areas and turbulence downstream of the deflector. This separation and recirculation contribute to energy losses in the form of heat and increase pressure losses. In a staggered configuration, deflectors are arranged in such a way that it forces the flow to follow a zigzag path. This creates multiple points of flow acceleration and deceleration, each point contributing to additional pressure losses, similar to the effect of steps. In addition to increasing pressure losses, the turbulence and recirculation areas, which are generated by square-edged deflectors and staggered configurations, have another important effect: noise generation.

Turbulence creates vortices and rapidly changing pressure fluctuations, which are significant sources of noise. These fluctuations are transmitted through the air as sound waves, the latter being perceived as a disturbing noise—the more intense the turbulence, the higher the generated noise level. Square-edged deflectors promote flow separation and the formation of strong turbulence, leading to significantly higher noise.

When using the flow fields, the broadband noise was computed. The acoustic field inside each analyzed configuration is shown in Figure 16.

Figure 16 illustrates the acoustic field and noise levels for different deflector configurations. The figure above triggers the following observations: The sharp-edged design causes flow separation at the deflector inlet, leading to recirculation areas and turbulence downstream, both generating noise. For the linear attenuator versions (Conf. I, Conf. II, and Conf. III), the sound power level of the acoustic sources does not show significant increases, with the primary noise sources being located near the leading edge of the baffle. In the case of the staggered attenuator variants (Conf. IV and Conf. V), the interaction of the upstream channel airflow with the leading edge of the downstream baffle amplifies the phenomenon downstream. The results of self-noise obtained with FEM simulation are presented in Table 2, showing that the triple-baffled staggered configuration is the noisiest option, despite this configuration obtaining the best results as far as noise attenuation is concerned.

According to Munjal [19] (Equation (3)), the resulting self-noise is 79.7 dB for single, double, and triple baffles because, in this formula, the length of the baffle is not considered, while taking into account the noise generated by the impact of air on the leading edge of the baffle, rather than the noise produced along the length of the blade or its trailing edge. In contrast, the FEM results are similar to the analytic ones and more reliable to be used in practice.

This study primarily aimed to evaluate various topologies of lamellar attenuators to be used in gas-turbine test stands, mainly from an acoustic perspective and under static

conditions. Although some flow conditions were introduced in the evaluation, the study did not actually include airflow testing. Further research should focus on conducting acoustic simulations under flow conditions. Additionally, optimizing the geometry of the attenuators by incorporating rounded leading and trailing edges on baffles could further enhance their flow performance, although important acoustic improvements are not expected to be obtained (acoustic attenuation is less dependent on geometric optimizations).

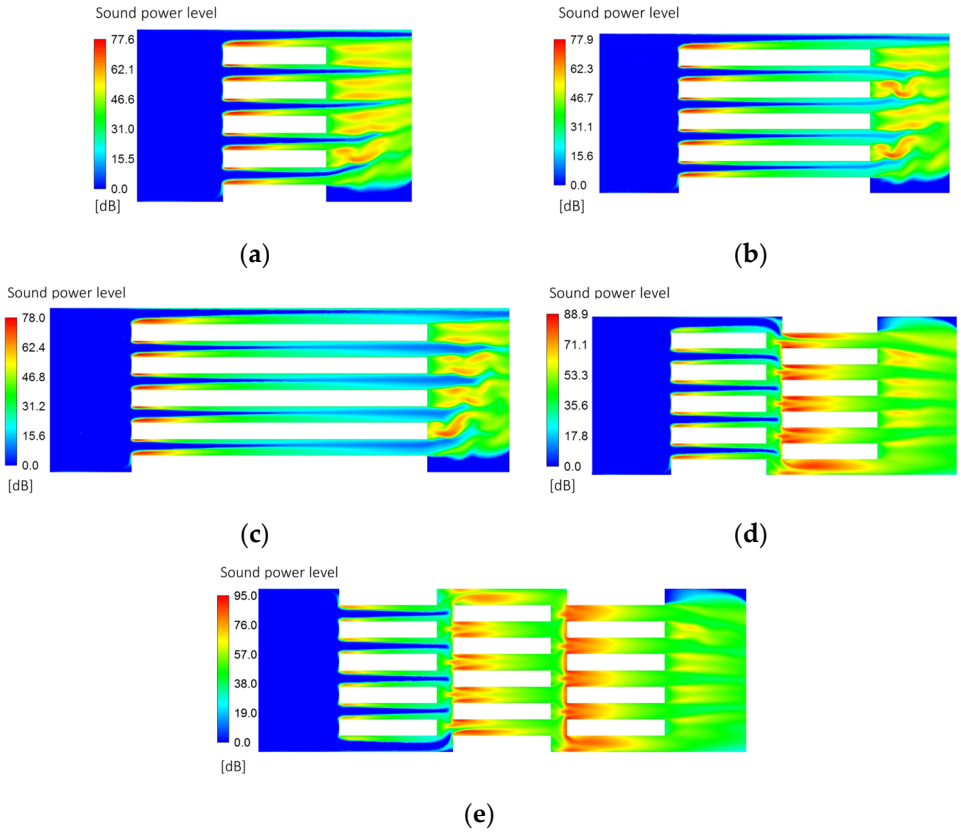

Figure 16. Noise induced by the flow inside the attenuator—Acoustic Power Level [dB]: (**a**) Conf. I—single baffled_linear configuration; (**b**) Conf. II—double baffled_linear config.; (**c**) Conf. III—triple baffled_linear; (**d**) Conf. IV—double baffled_staggered config.; (**e**) Conf. V—triple baffled_staggered config.

Table 2. Self-noise for each configuration—sound power level computed with FEM.

Configuration	Sound Power Level [dB]
Conf. I—single baffled_linear configuration	77.6
Conf. II—double baffled_linear	77.9
Conf. III—triple baffled_linear	78.0
Conf. IV—double baffled_staggered	88.9
Conf. V—triple baffled_staggered	98.0

7. Conclusions

This paper has undertaken a preliminary comprehensive analysis of sound attenuating methods used in silencer applications on gas-turbine test stands, thus addressing a critical need in the field of noise management for high-performance gas-turbine testing environments. The analysis of material parameters, design configurations, and integration techniques has provided us with a detailed framework for an effective design procedure for noise attenuators. While the study primarily focused on the static acoustic behavior of an attenuator, certain considerations were also made on flow conditions (without flow,

indirect, and reverse flow) while taking into consideration the influences of the convective effect on attenuation, by assessing the attenuation at different Mach numbers, pressure drops, and self-generated noise aspects to provide a broader perspective in choosing the best design configuration.

The study investigated various calculation methods for the evaluation of noise reduction in both linear and staggered baffles using a scaled-down model of an attenuator. Analytical methods and advanced computational techniques such as finite-element analysis were employed, along with an adapted and modified Embleton calculation method used for staggered baffle configurations, to predict the acoustic performance of various attenuator designs. It was concluded that the Embleton method, while widely used, tends to offer excessive and unrealistic values for linear configurations, prompting the need for modification, especially for staggered configurations. These simulations were complemented by experimental validations, the latter confirming the reliability and accuracy of the predicted outcomes. Embleton's method generally aligned with the attenuation curves, although a noticeable decrease in predicted attenuation was observed at higher frequencies. Experimental data revealed significant acoustic attenuation, even for configurations with linearly arranged baffles, particularly at frequencies exceeding 6 kHz. However, a discrepancy was noted between the central frequencies of the attenuation peaks obtained in our measurements and in Embleton's method, primarily due to the method's inability to account for variations in the density of the mineral wool used in the baffles. These differences were seen after finite-element parameter manipulations.

Finite-element numerical simulations exhibited a high degree of fidelity with experimental measurements, especially at high frequencies. For linearly arranged baffles, the simulations accurately reflected the measured attenuation levels. However, Embleton's analytic method tended to overestimate attenuation as the length of the attenuator increased. By contrast, staggered baffle configurations predicted higher attenuation values compared to our measurements. This disparity can be attributed to assumptions made in the CAD model regarding perfect baffle positioning, as well as the introduction of noise from collateral sound paths in staggered configurations. The comparison graph of average insertion loss indicates that a three-baffle staggered arrangement is the most suitable choice for noise attenuation in gas-turbine test-stand applications, although an increase in self-generated noise was observed in flow conditions. Additionally, comparisons of sound-pressure levels revealed that the staggered configuration provided more attenuated acoustic fields than the linear configurations.

Pressure-loss assessments demonstrated that linear configurations generally exhibited lower pressure losses as compared to the staggered configurations, which was also obvious. Staggered arrangements induced higher pressure losses due to increased flow complexity and the interactions between jets and deflector surfaces. The acoustic field analyses highlighted the impact of sharp-edged deflectors on flow separation, turbulence generation, and subsequent noise generation. The staggered configurations exacerbated these effects, leading to significantly higher noise levels than the linear arrangements.

Overall, this study provided new insights into the acoustic and aerodynamic performance of lamellar attenuators for gas-turbine test-stand applications. Further research should focus on acoustic simulations under more flow conditions and optimizing attenuator geometries for further enhancement of the performance with respect to flow characteristics.

Author Contributions: Conceptualization, L.C. and M.D.; methodology, M.D.; software, M.D.; validation, L.C. and M.D.; formal analysis, L.C.; investigation, L.C.; data curation, M.D.; writing—original draft preparation, L.C. and M.D.; writing—review and editing, L.C. and M.D.; visualization, M.D.; supervision, L.C. All authors have read and agreed to the published version of the manuscript.

Funding: This work was carried out through the Nuclear Program within the National Plan for Research, Development, and Innovation 2022–2027, conducted with the support of MCID, project no. PN23.12.01.01.

Institutional Review Board Statement: Not applicable.

Informed Consent Statement: Not applicable.

Data Availability Statement: The data presented in this study are available on request from the corresponding author. The data are not publicly available due to internal institutional restrictions.

Acknowledgments: The data presented and analyzed in this report were obtained with the help of INCDT COMOTI's Research and Experiments Center in the field of Acoustic and Vibrations staff and facility, and the work was carried out through the anechoic chamber and measurement equipment.

Conflicts of Interest: The authors declare no conflicts of interest. The funders had no role in the design of the study, in the collection, analyses, data interpretation, the writing of the manuscript, or in the decision to publish the results.

References

1. Ver, I.L.; Beranek, L. *Noise and Vibration Control Engineering. Principles and Applications*, 2nd ed.; John Wiley &Sons, Inc.: Hoboken, NJ, USA, 2006.
2. Bies, D.; Hansen, C. Flow resistance information for acoustical design. *Appl. Acoust.* **1980**, *13*, 357–391. [CrossRef]
3. Wang, C.; Li, C.; Hunag, L. Realization of a broadband low-frequency plate silencer using sandwich plates. *J. Sound Vib.* **2008**, *318*, 792–808. [CrossRef]
4. Erkan, D. *Duct Acoustics. Fundamentals and Applications to Mufflers and Silencers*; Cambridge University Press: Cambridge, UK, 2021.
5. Sumit, S.; Kumbhar, S.; Goilkar, S. Acoustics and Flow Field Analysis of Perforated Muffler Design. *Int. J. Eng. Dev. Res.* **2014**, *2*, 2321–9939.
6. Yu, X.; Cheng, L. Duct noise attenuation using reactive silencer with various internal configurations. *J. Sound Vib.* **2015**, *335*, 229–244. [CrossRef]
7. Wang, H.; Vardy, A.E.; Pokrajac, D. Pressure radiation from a perforated duct exit region. *J. Sound Vib.* **2015**, *351*, 29–42. [CrossRef]
8. Zhou, C.W.; Lainé, J.P.; Ichchou, M.N.; Zine, A.M. Numerical and experimental investigation on broadband wave propagation features in perforated plates. *Mech. Syst. Signal Process.* **2016**, *75*, 556–557. [CrossRef]
9. Williams, P.; Kirby, R.; Hill, J.; Åbom, M.; Malecki, C. Reducing low frequency tonal noise in large ducts using a hybrid reactive-dissipative silencer. *Appl. Acoust.* **2018**, *131*, 61–69. [CrossRef]
10. Terashima, F.J.H.; de Lima, K.F.; Barbieri, N.; Barbieri, R.; Filho, N.L.M.L. A two-dimensional finite element approach to evaluate the sound transmission loss in perforated silencers. *Appl. Acoust.* **2022**, *192*, 108694. [CrossRef]
11. Kalita, U.; Singh, M. Acoustic performance analysis of muffler by varying sound absorption materials. *Mater. Today* **2023**. [CrossRef]
12. Su, X. Acoustics of Parallel Baffles Muffler with Micro-Perforated Panels. *KTH Aeronaut. Veh. Eng.* 2011. Available online: https://kth.diva-portal.org/smash/record.jsf?pid=diva2:458126&dswid=6023 (accessed on 25 April 2024).
13. Liu, L.; Qio, Y.; Hao, Z.; Sheng, X. A modified time domain approach for calculation of noise reduction and acoustic impedance of intake duct system. *Appl. Acoust.* **2020**, *168*, 107420. [CrossRef]
14. Li, K.; Nenning, B.; Perrey-Debain, E.; Dauchez, N. Poroelastic lamellar metamaterial for sound attenuation in a rectangular duct. *Appl. Acoutics* **2021**, *176*, 107862. [CrossRef]
15. Bogdanovici, D. Calculation Methods for Predicting Attenuation of Parallel Baffle Type Silencers. Master's Thesis, Chalmers University of Technology, Gothenburg, Sweden, 2014.
16. Embleton, T.; Mufflers in Beranek, L. *Noise and Vibration Control*; Insitute for Noise Control Engeneering: Wakefield, MA, USA, 1971; pp. 362–405.
17. Ingard, K.U. *Notes on Sound Absorption Technology*; Polish Academy of Sciences: Warsaw, Poland, 1996.
18. Ray, E. *Industrial Noise Series VII*; Absorptive Silencer Design. Universal. 2010. Available online: https://www.yumpu.com/en/document/view/34871818/absorptive-silencer-design-universal-acoustic-silencers (accessed on 19 March 2024).
19. Munjal, M.L. *Acoustics of Ducts and Mufflers with Application to Exhaust and Ventilation System Design*; Wiley-Interscience: Hoboken, NJ, USA, 1987.
20. D'Udekem, D. Acoustic Simulations with ACTRAN. 2012. Available online: https://www.europages.com/filestore/gallery/a8/82/16231337_8117db89.pdf (accessed on 20 March 2024).
21. Sreeja, R. Delany-Bazley Model—A Powerful Tool in Optimizing the Acoustic Characteristics of Passive Fibrous Sound Absorbers for Noise Reduction Applications. *Int. J. Appl. Eng.* **2021**, *16*, 332–339.
22. Won, K.; Choe, J. Transmission loss analysis in a partitioned duct with porous boundaries based on combination of FEM and measurement of sound absorption coefficients. *Appl. Acoust.* **2020**, *165*, 107291. [CrossRef]
23. *ISO 3745*; Acoustics—Determination of Sound Power Levels and Sound Energy Levels of Noise Sources Using Sound Pressure—Precision Methods for Anechoic Rooms and Hemi-Anechoic Rooms. ISO: Geneva, Switzerland, 2012.
24. Available online: https://comoti.ro/en/acoustic-vibrations-laboratory/ (accessed on 5 April 2024).
25. Parker, R.; Welsh, M.C. Effects of sound on flow separation from blunt flat plates. *Int. J. Heat Fluid Flow* **1983**, *4*, 113–127. [CrossRef]

26. Yu, D.; Butler, K.; Kareem, A.; Glimm, J.; Sun, J. Simulation of the Influence of Aspect Ratio on the Aerodynamics of Rectangular Prisms. *J. Eng. Mech.* **2012**, *139*. [CrossRef]
27. Shoukry, A.; Mohany, A. Characteristics of the flow-induced noise from rectangular rods with different aspect ratios and edge geometry. *J. Fluids Struct.* **2023**, *122*, 103959. [CrossRef]
28. Tang, S.K. Duct sound produced by vortex flow over a splitter plate. *J. Sound Vib.* **2022**, *541*, 117352. [CrossRef]
29. Zhang, X.; Cheng, L. Acoustic silencing in a flow duct with micro-perforated panel liners. *Appl. Acoust.* **2020**, *167*, 107382. [CrossRef]
30. Proudman, I. The generation of noise by isotropic turbulence. *Proc. R. Soc. Lond.* **1952**, *214*, 119–132.
31. Cai, C.; Mak, C.M. Generalized flow-generated noise prediction method for multiple elements in air ducts. *Appl. Acoust.* **2018**, *135*, 136–141. [CrossRef]
32. MSC Software Company. Actran Software—A Finite Element-Based Computer Aided Engineering Software Modeling the Acoustic Behavior of Mechanical Systems and Parts. Version 19.

Disclaimer/Publisher's Note: The statements, opinions and data contained in all publications are solely those of the individual author(s) and contributor(s) and not of MDPI and/or the editor(s). MDPI and/or the editor(s) disclaim responsibility for any injury to people or property resulting from any ideas, methods, instructions or products referred to in the content.